This is the peer reviewed version of the following article: W. Zheng, Y. Li, M. Liu, C.-S. Tsang, L. Y. S. Lee, K.-Y. Wong, Cu2+-doped Carbon Nitride/MWCNT as an Electrochemical Glucose Sensor. Electroanalysis 2018, 30, 1446–1454, which has been published in final form at https://doi.org/10.1002/elan.201800076.

Cu^{2+}-doped Carbon Nitride/MWCNT as an Electrochemical Glucose Sensor

Weiran Zheng,[1] Yong Li,[1] Mengjie Liu, Chui-Shan Tsang, Lawrence Yoon Suk Lee, Kwok-Yin Wong**

Department of Applied Biology and Chemical Technology and the State Key Laboratory of Chirosciences, The Hong Kong Polytechnic University, Hung Hom, Kowloon, Hong Kong, China

[1] These authors contributed equally to this work.
* e-mails: lawrence.ys.lee@polyu.edu.hk; kwok-yin.wong@polyu.edu.hk

Received:
Accepted:

Abstract
The rational design of electrocatalysts with abundant active sites and high conductivity is the key to the development of glucose sensors. Herein, we report the preparation of a Cu^{2+}-doped C_3N_4 supported on multi-walled carbon nanotube (MWCNT) network (Cu^{2+}-C_3N_4/MWCNT) as a highly efficient non-enzymatic glucose sensing system. The morphologic and structural investigations using TEM, AFM, XRD, XPS, EPR, and *i*-V response indicate the successful insertion of Cu^{2+} into the C_3N_4 *inter*-layers *via* an out-of-plane on-top configuration and the consequent exfoliation of C_3N_4 layers without forming CuO or $Cu(OH)_2$. Such material can act as an electrocatalyst for glucose electrooxidation, and MWCNT can greatly reduce the charge transfer resistance and enhances activity. An optimised Cu^{2+} doping level (12 wt%) in Cu^{2+}-C_3N_4/MWCNT was established to realise high sensitivity towards glucose sensing (929 mA/M cm^2), large linear range (0.5 μM ~ 12 mM), low detection limit (0.35 μM), and short response time (< 3s). Excellent selectivity against the interferents, such as dopamine, ascorbic acid, sucrose, and lactose, is also observed. In the blood serum tests, as-prepared glucose sensor reports comparable and reproducible results, demonstrating its practical potentials.

Keywords: C_3N_4, copper ion, glucose sensor, MWCNT, electrocatalysis

DOI: 10.1002/elan

1. Introduction

The development of highly efficient glucose electrooxidation catalyst as glucose sensors has been under the spotlight of research for decades due to its broad application in medical diagnosis, fuel cell, and biomass conversion.[1] Two types of glucose sensor have been developed to date: enzymatic and non-enzymatic sensors.[2] Enzymatic glucose sensors are among the earliest systems studied and commonly involve the use of immobilised glucose oxidase. However, the use of enzyme raises the problems of high cost and structural instability. Moreover, the temperature, humidity, pH, and toxic chemicals can affect their activity.[3] Such problems lead to the development of non-enzymatic glucose sensors.

Copper-based nanomaterials (Cu,[4,5] CuO,[6,7] Cu-MOF,[8] Cu_2O,[9] *etc.*) have been reported to show considerable electrocatalytic activities towards glucose electrooxidation. The commonly accepted mechanism involves two steps: 1. Electrooxidation of surface Cu(II) species to Cu(III) species; 2. Redox reaction between Cu(III) species and adsorbed glucose, regenerating Cu(II) sites.[10] Thus, a suitable glucose sensor needs a large population of surface Cu(II) as well as high electronic conductivity. Based on such guidelines, extensive efforts have been made, for example reducing the particle size,[4] altering the morphology,[11,12] and changing the catalyst support.[13–15] We recently found that Cu^{2+} species alone can act as an ultra-efficient homogeneous electrocatalyst for glucose electrooxidation, achieving high atomic efficiency.[16] Although such homogeneous system is not practical for real device fabrication, it posed the insights that conductive support with abundant surface-anchored Cu^{2+} ions would make a good glucose sensor.

Graphitic carbon nitride (g-C_3N_4) is a suitable support material due to its layered structure and rich N atoms on the surface for Cu^{2+} coordination.[17] Vázquez-González *et al.* reported a simple sonication process to prepare Cu^{2+}-modified C_3N_4 nanoparticles.[18] However, the semiconductivity of C_3N_4 limits its direct application in electrocatalysis. It is thus reasonable to introduce another conductive support, such as multi-walled carbon nanotubes (MWCNT), to increase the conductivity while maintaining the advantage of C_3N_4 as Cu^{2+} anchoring sites.

In this paper, we prepared a Cu^{2+}-doped C_3N_4 supported on MWCNT (Cu^{2+}-C_3N_4/MWCNT) using ultrasonication process. The morphology and structure of such composite were studied combining several microscopic and diffraction techniques. The glucose electrooxidation activity was investigated using the Cu^{2+}-C_3N_4/MWCNT catalyst of different Cu^{2+} doping level and MWCNT content. Finally, the glucose sensor properties of as-prepared catalyst were discussed in detail with respect to sensitivity, linear response range, detection limit, response time, interference study, and blood serum testing.

2. Experimental section

2.1. Chemicals

Urea (98%), D-(+)-glucose (>99.5%), multi-walled carbon nanotube (>95%, 6-9 nm × 5μm), Nafion perfluorinated ion-exchange resin (5 wt%), and copper(II) nitrate (98%) were purchased from Sigma-Aldrich. Sodium hydroxide (>96%) was purchased from UNI-CHEM. All chemicals were used without further purification. All aqueous solution was prepared using double deionised water (DI water) from MilliQ water System (Millipore, USA, R>18.2 MΩ/cm).

2.2. Preparation of Cu^{2+}-C_3N_4

C_3N_4 was prepared by the pyrolysis of urea according to the procedure previously reported.[19] In a typical process, 20 g of urea was placed in a crucible with a cover and heated up to 350 °C for 2 h with a heating rate of 10 °C min^{-1} in the N_2 atmosphere. Further treatment at 550 °C for another 2 h yielded yellow powder as product.

The Cu^{2+}-C_3N_4 was prepared by mixing C_3N_4 and $Cu(NO_3)_2$ aqueous solution under ultrasonication conditions at room temperature (Cole-Parmer 130-Watt Ultrasonic Processors). Briefly, 25 mg of C_3N_4 was ultrasonicated in 25 mL DI water for 30 min until a stable light-yellow suspension was obtained. Then, a pre-determined amount of 0.1 M $Cu(NO_3)_2$ aqueous solution was added to the suspension to achieve different Cu^{2+}/C_3N_4 ratio. The mixed solution was ultrasonicated for another 30 min to allow sufficient interaction between Cu^{2+} ion and C_3N_4. The as-prepared solution was named as Cu^{2+}(m wt%)-C_3N_4 (m = 1, 9, 12, 17, 29, 50) for clarification.

2.3. Preparation of Cu^{2+}-C_3N_4/MWCNT

For the preparation of Cu^{2+}-C_3N_4/MWCNT, various amounts of MWCNT were added to the mixed solution of Cu^{2+}-C_3N_4. The mixture was ultrasonicated for 1 h until a stable suspension was obtained. To clarify, this composite was named as Cu^{2+}(m wt%)-C_3N_4/(n wt%)MWCNT (n = 5 and 10).

2.4. Characterization

X-ray diffraction (XRD) patterns were collected on a SmartLab X-ray diffractometer (Rigaku) operated with Cu-K_α (λ = 1.5418 Å) from a generator operating at 45 kV and 200 mA. Transmission electron microscopic (TEM) images were taken by a STEM (JEOL model JEM-2100F). Atomic force microscopy (AFM) images were obtained from a Bruker Multimode 8-HR AFM using PeakForce Tapping mode with the SNL-10 cantilever. X-ray photoelectron spectroscopy (XPS) analysis of the material was carried out using a Thermo Fisher ESCALAB 250Xi. Electron paramagnetic resonance (EPR) spectra were obtained from an ADANI SPINSCAN X EPR (ESR) X-band spectrometer with operating microwave frequency of 9.390 GHz at room temperature. The conductivity test (current-voltage test or i-V test) was carried out on a Keithley 4200A-SCS semiconductor analyser using a two-point probe system. The powder sample was pressed into a solid sheet, and two probes were placed in contact with the surface of the sheet. The voltage bias was set to be -1.0 ~ 1.0 V.

2.5. Preparation of modified electrodes

Glassy carbon electrode (GCE) was used for surface modification. A GCE (d = 3 mm, surface area = 0.07 cm^2) was first polished with 1.0, 0.3, and 0.05 μm α-Al_2O_3 powders (CH Instruments), followed by rinsing with DI water and acetone. The cleaned GCE was dried in air at room temperature. 20 μL of the prepared suspension (C_3N_4 concentration is 1 mg/mL in all samples) of Cu^{2+}-C_3N_4 and Cu^{2+}-C_3N_4/MWCNT was drop-cast on the GCE surface and air-dried at room temperature for 3 h.

2.6. Electrochemical measurements

Cyclic voltammetry (CV) and amperometry experiments were performed on a CHI 760E electrochemical analyser (CH Instruments, Inc.). Electrochemical impedance spectroscopic (EIS) measurements were obtained from a PARSTAT MC-PMC1000 (Princeton Applied Research, AMETEK Inc.) electrochemical system. All measurements were performed in 10 mL of 0.1 M NaOH aqueous solution using the three-electrode system. Saturated calomel electrode (SCE) was used as the reference electrode and Pt wire as the counter electrode. Before the CV and amperometric studies, the modified electrodes were first swept within the potential range of 0 ~ 0.7 V (*vs.* SCE, same below) until a stable current was reached. The CV plots were obtained with a scan rate of 5 mV/s. Amperometric measurements were taken at 0.6 V with continuous stirring at 780 rpm. Aliquots of glucose solution were injected every 50 s after the background current stabilised. Electrochemical impedance spectroscopy (EIS) was carried out at 0.6 V within a frequency range of 1 MHz ~ 50 mHz and amplitude of 10 mV RMS.

3. Results and discussion

3.1. Morphology of Cu^{2+}-C_3N_4 and Cu^{2+}-C_3N_4/MWCNT

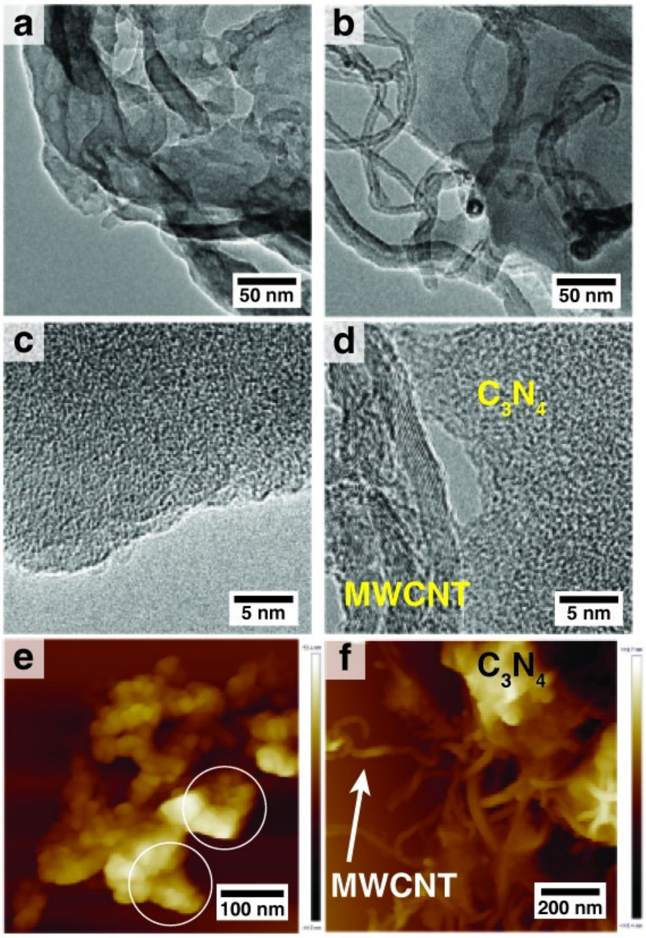

Fig. 1. Morphology of Cu^{2+}(12 wt%)-C_3N_4: (a) TEM image, (c) HRTEM image, (e) AFM image; Cu^{2+}(12 wt%)-C_3N_4/(5 wt%)MWCNT: (b) TEM image, (d) HRTEM image, (f) AFM image.

Fig. 1a and b show the TEM images of Cu^{2+}(12 wt%)-C_3N_4 and Cu^{2+}(12 wt%)-C_3N_4/(5 %)MWCNT. A typical graphitic morphology of as-prepared C_3N_4 agrees well with the previous report,[19] and confirms its layered platelet-like morphology (g-C_3N_4). Mixing with MWCNT produces the highly-dispersed nanotube composites found in the high-resolution TEM (HRTEM) images of both materials (Fig. 1c and d). No nanoparticle structure of CuO or $Cu(OH)_2$ is evident. It is thus possible that Cu^{2+} ions are coordinated to the C_3N_4 surface in atomic/ionic form. The multi-wall structure in contact with C_3N_4 can be observed in Fig. 1d. The corresponding AFM images of both materials are shown in Fig. 1e and f where the aggregation of C_3N_4 to nanoparticle cluster as well as layered structure (circles in Fig. 1e) is confirmed. After the MWCNT addition, C_3N_4 is found to integrate with the nanotube structure (Fig. 1f). Thus, after the ultrasonication process, Cu^{2+}, MWCNT, and C_3N_4 can form a composite structure of Cu^{2+}-C_3N_4/MWCNT.

3.2. Physical properties of Cu^{2+}-C_3N_4 and Cu^{2+}-C_3N_4/MWCNT

The crystalline structures of Cu^{2+}-C_3N_4 and Cu^{2+}-C_3N_4/MWCNT composites were studied using XRD, and the results are shown in Fig. 2a. Two characteristic peaks of graphitic C_3N_4 are found at 13.3° (d spacing = 6.65 Å) and 27.3° (d spacing = 3.27 Å), which can be assigned to the (100) and (002) planes.[17] Fig. 2c shows the structural illustration of C_3N_4 with its (100) and (002) plane exposed. The d spacing value of (100) and (002) planes are related to the *intra*-layer and *inter*-layer distances, respectively. After Cu^{2+} doping, a new peak evolves at 21.4° (d spacing = 4.15 Å), in addition to the existing (100) and (002) peaks. Such new peak is due to the structural disorder of C_3N_4 caused by Cu^{2+} doping. It is possible that Cu^{2+} ion can enter the *inter*-layer and coordinate with N atoms in-between (Fig. 2c), resulting in a longer (002) distance.

The degree of exfoliation of graphitic C_3N_4 can be estimated by the intensity ratio of (100) and (002) peaks, I_{100}/I_{002}.[17,20] A higher I_{100}/I_{002} ratio indicates the relative decrement of (002) plane signal compared to (100) plane, thus the fewer C_3N_4 layers. The intensity ratio for C_3N_4, Cu^{2+}-C_3N_4, and Cu^{2+}-C_3N_4/MWCNT are 0.29, 0.38, and 0.42, respectively, which suggests that the Cu^{2+} doping process leads to the partial exfoliation of bulk C_3N_4 to smaller particles, as shown in Fig. 2c.

XPS technique was employed to analyse the surface species and doping mechanism of Cu^{2+}-C_3N_4. Three samples were studied, including C_3N_4, Cu^{2+}(12 wt%)-C_3N_4, and Cu^{2+}(12 wt%)-C_3N_4/(5 wt%)MWCNT Fig. 2b shows the N 1s, C 1s, and Cu $2p_{3/2}$ regional comparison of the samples. For C_3N_4, the regional spectrum of C 1s presents a broad peak which can be further deconvoluted to three peaks at 398.4, 399.4, and 400.8 eV, which can be assigned to the N species in C-N-C, tertiary N-(C)$_3$, and N-H, respectively.[21] The surface distribution of N species can be estimated by the normalised deconvoluted peak area (total N peak area = 1), namely 0.58, 0.29, and 0.13 for C-N-C, tertiary N-(C)$_3$, and N-H. After Cu^{2+} doping, the peak positions of N species in both C-N-C and N-H are unchanged, while the binding energy of N-(C)$_3$ shifts to 399.6 eV. It is thus suggested that Cu^{2+} interacts mainly with N atoms in N-(C)$_3$ structure (electrons donated from N to Cu). Moreover, the relative peak area increases from 0.29 to 0.32 upon Cu^{2+} doping. It is possible that more N-(C)$_3$ units are exposed to the surface after introducing Cu^{2+}. (Figure 2c) However, it is interesting to find that the peak positions of all N species in Cu^{2+}-C$_3$N$_4$/MWCNT are identical to that in C$_3$N$_4$. It is possible that electron-rich MWCNT compensates the binding energy shift caused by electronic interaction between Cu^{2+} and N-(C)$_3$. With MWCNT introduced, the proportion of N-(C)$_3$ further increases to 0.45, showing the stabilisation effect of MWCNT to C$_3$N$_4$ nanoparticles. The existence of three C species is observed in C 1s XPS spectra of both C$_3$N$_4$ and Cu^{2+}-C$_3$N$_4$: C-C and/or adventitious carbon (284.9 eV), C-N-C (286.1 eV), and C-(N)$_3$ (288.0 eV).[21,22] No significant peak shift is observed, indicating that C atoms are not in direct contact with Cu^{2+}. After MWCNT addition, apart from the existing three C species, a new peak located at 284.1 eV evolves. It can be assigned to the sp^2 C species in the C=C structure of MWCNTs.[23] The Cu 2p$_{3/2}$ regional spectra of Cu^{2+}-doped samples (Cu^{2+}-C$_3$N$_4$ and C^{2+}-C$_3$N$_4$/MWCNT) show two peaks at 933.8 eV and 942.8 eV, which can be attributed to Cu(II) species and its well-known shake-up satellite peak.[24] It shows that only one form of Cu(II) species exists in the Cu^{2+}-doped C$_3$N$_4$ samples.

Based on the XPS results, it is reasonable to assume that Cu^{2+} ion interacts with C$_3$N$_4$ with the configuration shown in Fig. 2d: N atoms in N-(C)$_3$ share electrons with the on-top Cu^{2+} ions.

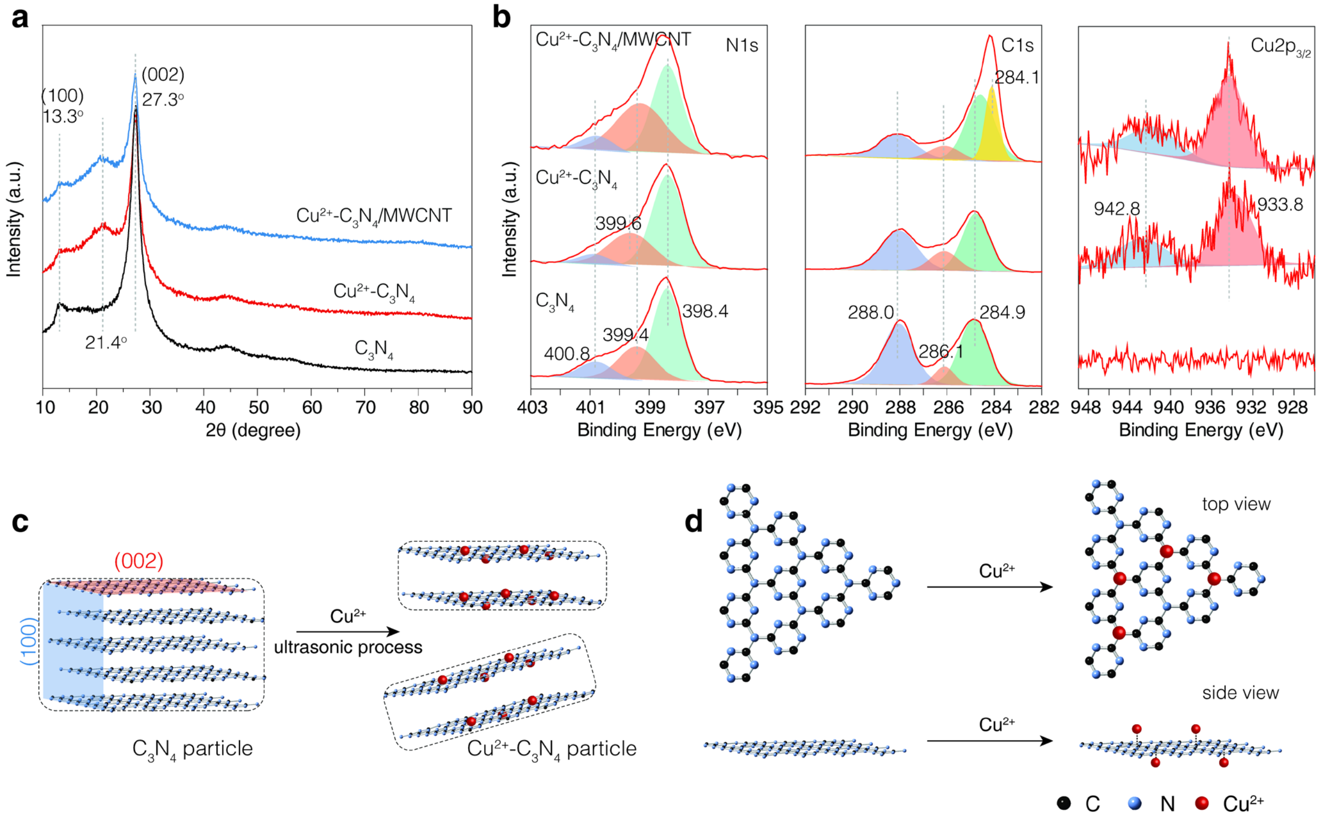

Fig. 2. (a) XRD patterns of C$_3$N$_4$, Cu^{2+}(12 wt%)-C$_3$N$_4$, and Cu^{2+}(12 wt%)-C$_3$N$_4$/(5 wt%)MWCNT; (b) XPS spectra of C$_3$N$_4$, Cu^{2+}(12 wt%)-C$_3$N$_4$, and Cu^{2+}(12 wt%)-C$_3$N$_4$/(5 wt%)MWCNT in the region of N 1s, C 1s, and Cu 2p$_{2/3}$. (c) Illustration showing the structural evolution of C$_3$N$_4$ during Cu^{2+} doping process; (d) The structural illustration of Cu^{2+} ion doping on C$_3$N$_4$ *via* an out-of-plane on-top interaction mode (top view and side view).

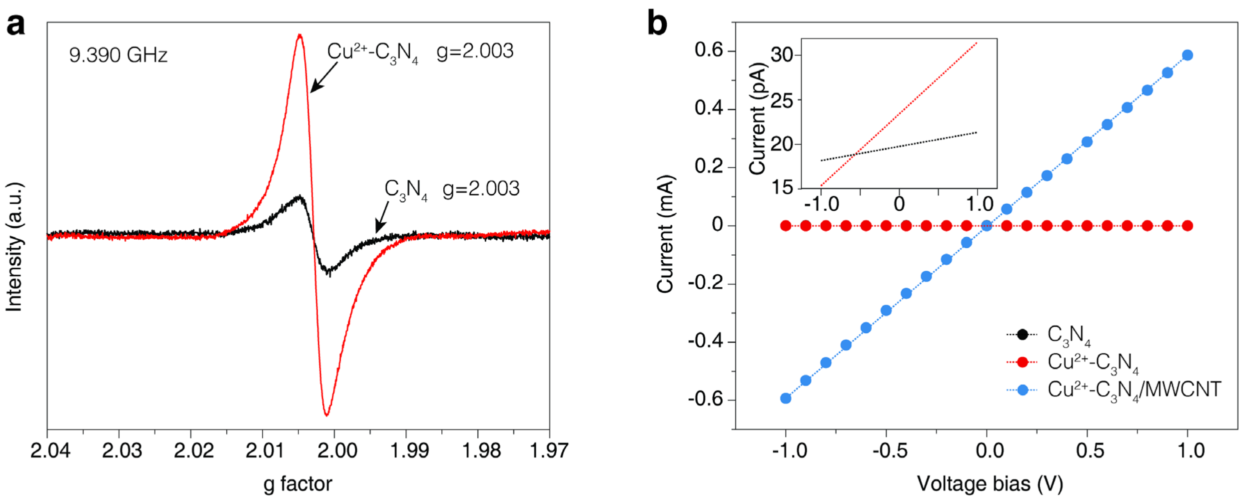

Fig. 3. (a) The X-band EPR spectra of C_3N_4 and Cu^{2+}(12 wt%)-C_3N_4; (b) The *i*-V curves of C_3N_4, Cu^{2+}(12 wt%)-C_3N_4, and Cu^{2+}(12 wt%)-C_3N_4/(5 wt%)MWCNT. Inset shows the magnified *i*-V curves of C_3N_4 and Cu^{2+}(12 wt%)-C_3N_4.

The electronic structures of C_3N_4 and Cu^{2+}-C_3N_4 were further studied by X-band solid-state EPR at room temperature, and the results are shown in Fig. 3a. Pure C_3N_4 shows a symmetrical signal centred at $g = 2.003$, which can be assigned to the unpaired electron of the π-bonded aromatic rings.[25] The EPR intensity of Cu^{2+}-doped C_3N_4, however, is significantly enhanced with same g factor, similar to the reported Fe^{3+}-doped C_3N_4.[26] Therefore, the introduction of Cu^{2+} generates delocalizing spins and results in a higher electron density and higher conductivity. The EPR spectrum of MWCNT-modified sample cannot be obtained due to the microwave adsorption property of MWCNT.

The *i*-V curves of C_3N_4, Cu^{2+}-doped C_3N_4, and Cu^{2+}-C_3N_4/MWCNT are shown in Fig. 3b. A two-probe system was used to measure the current-voltage response of the samples with voltage bias between -1 ~ 1 V. The slope values of the *i*-V curves can be used to estimate the conductivity. Semiconducting C_3N_4 shows a slope of 1.85×10^{-12} A/V, while Cu^{2+}-C_3N_4 shows a higher value of 8.06×10^{-12} A/V. Such results agree with the EPR results that Cu^{2+} doping process can increase the charge carrier density. Upon MWCNT modification, the slope value dramatically rises to 5.85×10^{-4} A/V, suggesting that MWCNT can lift the conductivity of Cu^{2+}-C_3N_4 by nearly 7.4×10^{7} times.

3.3. Cyclic voltammetry study of Cu^{2+}-C_3N_4 and Cu^{2+}-C_3N_4/MWCNT

The electrocatalytic property of Cu^{2+}-doped C_3N_4 was studied by potential stripping of the modified GCE in alkaline electrolyte. Fig. 4a shows the CV plots of C_3N_4 and Cu^{2+}(12 wt%)-C_3N_4 in 0.1 M NaOH electrolyte with and without 5 mM glucose. As illustrated, bare C_3N_4 shows a pair of redox peaks which can be associated with the surface functionalization of N sites by OH^- species.[27] The CV remains similar after the addition of glucose, indicating that C_3N_4 is inactive toward glucose electrooxidation. With the C_3N_4 doped with Cu^{2+} ions, the current density (*j*) of the CV decreases dramatically, suggesting a decrease in the double layer capacitance. The possible reason is that the N atom sites have been occupied by Cu^{2+} ion, leaving only a few of them available for OH^- adsorption/desorption. With glucose addition, a broad electrooxidation peak appears at 0.6 V, evidently the electrooxidation signal of glucose. The possible mechanism is illustrated in Fig. 4b. Similar to the mechanism we proposed for glucose electrooxidation using homogeneous Cu^{2+} ion,[16] the Cu^{2+}-C_3N_4 is first oxidised to Cu^{3+}-C_3N_4, then glucose reacts with Cu^{3+} species, producing gluconic acid and regenerating the Cu^{2+} species.

The surface area of C_3N_4 is the limiting factor for hosting Cu^{2+} ions. To determine the doping amount effect, samples of C_3N_4 were doped with different amount of Cu^{2+} and their electrocatalytic activities are tested (Fig. 4c). All Cu^{2+}-C_3N_4 samples gave rise to the glucose electrooxidation peak at *ca.* 0.6 V. With the Cu^{2+} wt% increases from 1 to 12%, the peak current density steadily increases. Such increment is associated with the number of total available active sites (Cu^{2+}). However, when the Cu^{2+} weight percentage was further increased over 12%, the peak current density decreases. This suggests that the surface sites available for hosting Cu^{2+} are saturated at 12% Cu^{2+}. Further addition of Cu^{2+} would only increase weakly adsorbed Cu^{2+} *via* electrostatic force, which forms a semiconducting $Cu(OH)_2$ layer in the NaOH electrolyte, suggested by high resistance values.

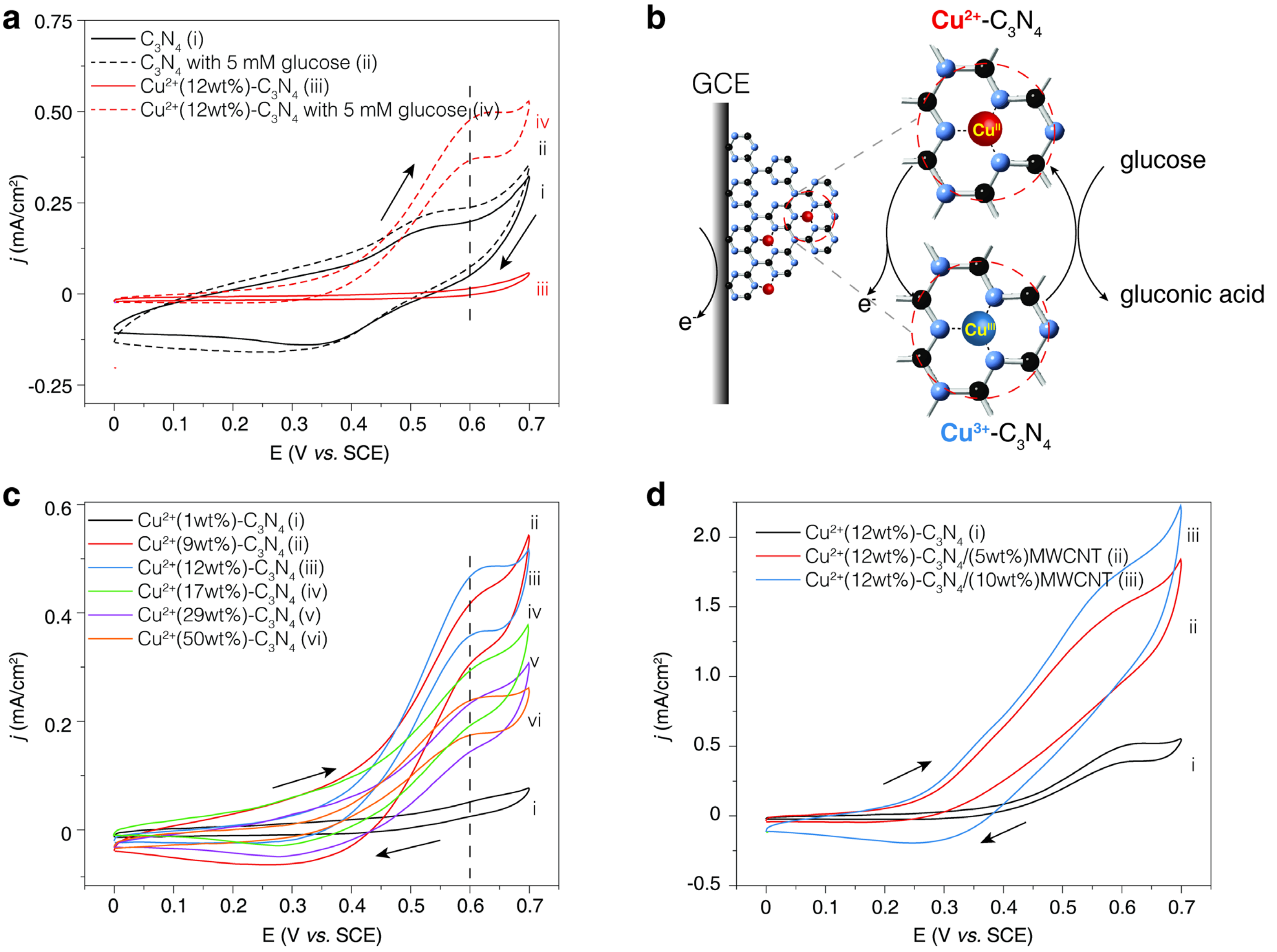

Fig. 4. (a) CV plots of C_3N_4 and Cu^{2+}(12 wt%)-C_3N_4 in 0.1 M NaOH solution without and with 5 mM glucose; (b) Illustration of the glucose electrooxidation mechanism on Cu^{2+}-C_3N_4; (c) CV plots of Cu^{2+}(*m* wt%)-C_3N_4 in 0.1 M NaOH solution containing 5 mM glucose. (d) CV plots of Cu^{2+}(12 wt%)-C_3N_4 and Cu^{2+}(12 wt%)-C_3N_4/MWCNT. Scan rate is 5 mV/s.

Based on the *i*-V tests shown in Fig. 3b, we confirmed the MWCNT can significantly increase the conductivity of the C_3N_4 composite. Thus, MWCNT was introduced as secondary support for C_3N_4. Fig. 4(d) compares the CV plots after 5 wt% and 10 wt% of MWCNT are introduced to Cu^{2+}(12 wt%)-C_3N_4. After the MWCNT addition, the oxidation peak current density increases nearly 3.2 (5% MWCNT) and 4 (10% MWCNT) times compared to that of original Cu^{2+}(12 wt%)-C_3N_4 catalyst. Such results suggest that MWCNT enhances the catalytic activity of Cu^{3+}-C_3N_4 by providing a conductive framework.

3.4. EIS study of Cu^{2+}-C_3N_4 and Cu^{2+}-C_3N_4/MWCNT

The EIS of Cu^{2+}(12 wt%)-C_3N_4 and Cu^{2+}(12 wt%)-C_3N_4/MWCNT also support the enhanced conductivity by MWCNT support in electrocatalytic conditions. The corresponding Nyquist plots are shown in Fig. 5. With the potential of 0.6 V, Cu^{2+}(12 wt%)-C_3N_4 shows the highest charge transfer resistance (11,372 Ω) towards glucose electrooxidation. After adding 5% MWCNT, the resistance decreases to 5,292 Ω. Further resistance reduction to 2,612 Ω can be achieved by introducing 10% MWCNT. Both CV and EIS results agree well on that the incorporation of MWCNT to Cu^{2+}-C_3N_4 can promote the glucose electrooxidation by reducing the charge transfer resistance. These data are also consistent with the EPR and *i*-V test results.

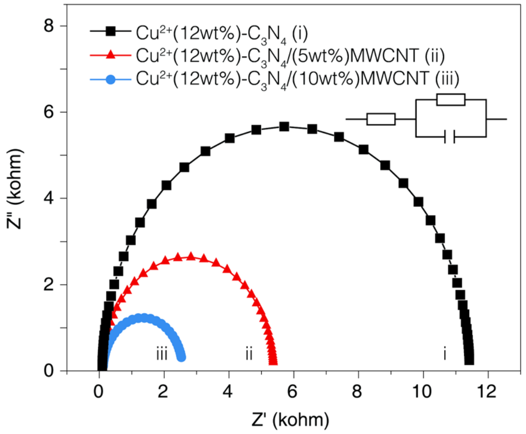

Fig. 5. Nyquist plots of Cu^{2+}(12 wt%)-C_3N_4 and Cu^{2+}(12 wt%)-C_3N_4/MWCNT in 0.1 M NaOH containing 5 mM glucose. The applied potential is 0.6 V. The data points are fitted with Randles circuit.

3.5. Amperometry study

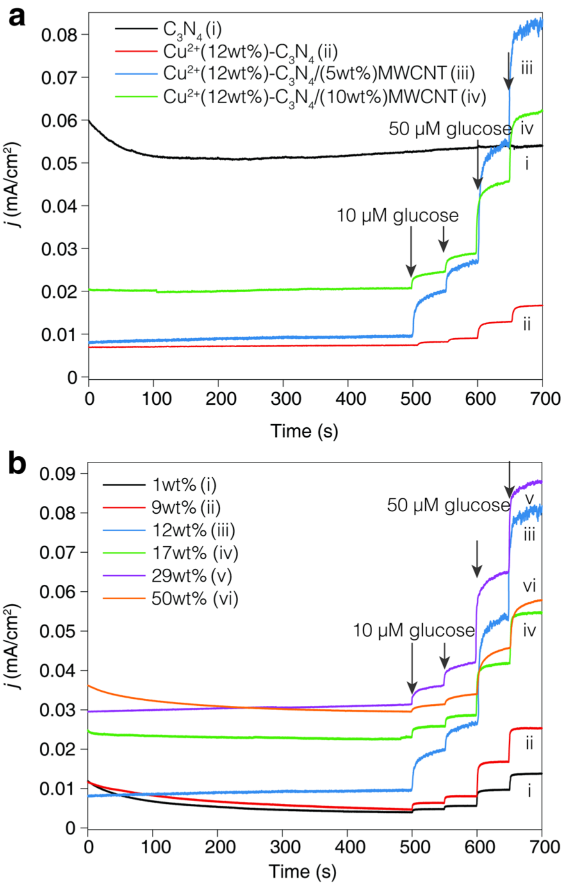

Fig. 6. (a) Amperometric *i*-t response curves of C_3N_4, Cu^{2+}(12 wt%)-C_3N_4 and Cu^{2+}(12 wt%)-C_3N_4/MWCNT; (b) Amperometric *i*-t response curves of Cu^{2+}(*m* wt%)-C_3N_4/(5 wt%)MWCNT (*m* = 1, 9, 12, 17, 29, 50). Inserted values are the glucose concentration changes at different time mark. The applied potential is 0.6 V.

The modified GCEs were further used to study the current responses for the successive injection of glucose to 0.1 M NaOH solution at an applied potential of 0.6 V. To find out the optimal MWCNT concentration, C_3N_4 and Cu^{2+}(12 wt%)-C_3N_4 mixed with 5 % and 10 % MWCNT are studied first and the results are shown in Fig. 6a. At an applied potential of 0.6 V, the background current stabilises after 500 s for all modified GCEs. C_3N_4 shows no current response to the glucose addition while Cu^{2+}-doped C_3N_4 and C_3N_4/MWCNT exhibit the increase of the current density with glucose concentration. The sensitivity values calculated based on *i*-t curves are 78, 929, and 348 mA/M cm^2 for Cu^{2+}(12 wt%)-C_3N_4, Cu^{2+}(12 wt%)-C_3N_4/(5 wt%)MWCNT, and Cu^{2+}(12 wt%)-C_3N_4/(10 wt%)MWCNT, respectively. The highest sensitivity is observed with 5 wt% MWCNT, not 10 wt% MWCNT. The excessive amount of MWCNT is believed to interrupt the mass transfer of glucose to the Cu^{2+} sites, thus reduces the sensitivity.

Fig. 6b shows the effect of Cu^{2+} doping level to the sensitivity. For 10 μM glucose concentration changes, 12 wt% Cu^{2+}-doped C_3N_4/(5 wt%)MWCNT shows the highest current response. Similar to the findings in Fig. 4c, it is possible that the Cu^{2+} doping level higher than 12% would cause higher resistance due to the formation of $Cu(OH)_2$ layers on C_3N_4.

3.6. Sensor properties study: linear range, interference resistance, and detection limit

For the development of a practical electrochemical glucose sensor, several key properties are required to be evaluated, including linear range, interference resistance, and detection limit. As indicated by the amperometry studies, the highest sensitivity value of 929 mA/M cm^2 is achieved by using Cu^{2+}(12 wt%)-C_3N_4/(5 wt%)MWCNT as a glucose sensor. The linear range study is shown in Fig. 7a. Different glucose concentration changes are introduced to the electrolyte, and the current density is plotted against glucose concentration. Two linear ranges are evident: 0.5 μM ~ 3.5 mM and 3.0 ~ 12 mM (inset in Fig 6a). The correlation coefficient R^2 is calculated to be 0.9993 and 0.9967, respectively, indicating an excellent correlation between current and glucose concentration. The formation of two regions implies that the different kinetic control steps are involved. At low glucose concentrations, mass transfer of glucose determines the reaction rate, whereas at the higher glucose concentrations, charge transfer to glucose does. The calculated detection limit is 0.35 μM (S/N = 3) and the response times are < 3s. Regarding all the properties important for the sensor, our Cu^{2+}-C_3N_4/MWCNT system shows excellent performances, which is comparable, if not better, to other Cu-based non-enzymatic glucose sensors (Table 1). To determine the blood glucose level, it is also important for the electrocatalyst to resist the interfering species in blood, such as dopamine, ascorbic acid, sucrose, and lactose. Fig. 7b shows the interference study with 10 μM of various interferents. Compared to the major current response due to glucose, there is an only minor increment in current density in response to the interferents, an indication of superior selectivity of Cu^{2+}-C_3N_4/MWCNT to glucose oxidation and resistance to surface poison.

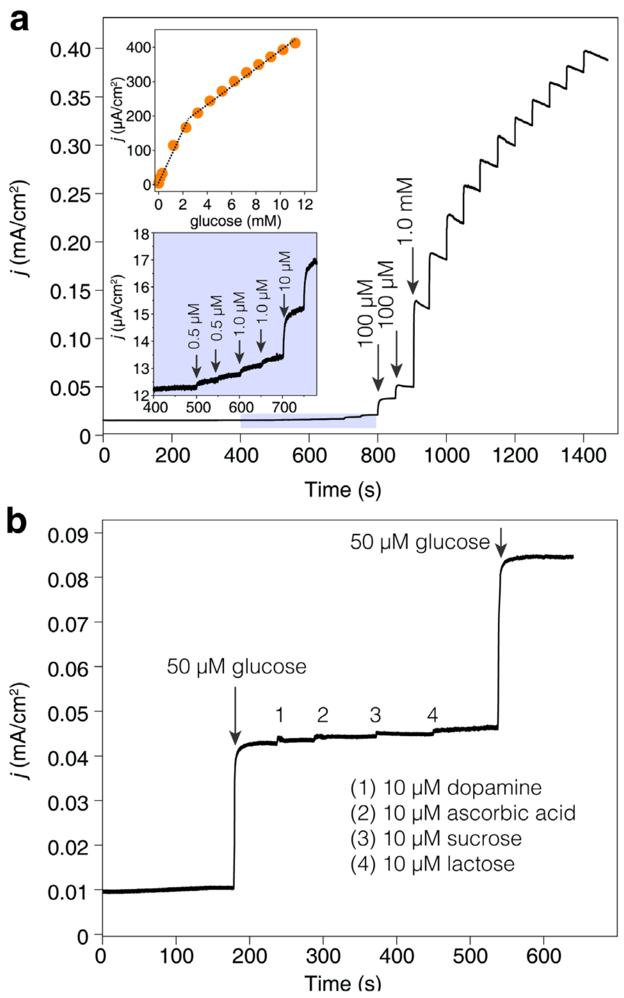

Fig. 7. (a) Amperometric *i*-t response curve of Cu^{2+}(12 wt%)-C_3N_4/(5 wt%)MWCNT to the successive injection of glucose. The inserted values show the glucose concentration change. The inset on top is the calibration curve for glucose detection, and the inset on bottom is the enlarged *i*-t curve between 400 and 780 s; (b) Interference experiment of Cu^{2+}(12 wt%)-C_3N_4/(5 wt%)MWCNT in 0.1 M NaOH with the injections of glucose (50 μM) and interferents (dopamine, ascorbic acid, sucrose, and lactose; 10 μM).

Table 1. Performance comparison of Cu-based non-enzymatic electrochemical glucose sensors.

Electrode	Sensitivity (mA/M cm^2)	Detection limit (μM)	Linear range (mM)	Ref.
Cu NPs/GO/SWCNT	930	0.34	0.001-4.5	[28]
CuO NPs/G	1,065	1.0	0.001-8	[29]
CuO NPs	404	1.0	0.001-2.55	[8]
CuO nanorods/graphite	371	4	0.004-8	[30]
Cu-MOF	89	0.01	0.06-5	[31]
Cu^{2+}-C_3N_4/MWCNT	929	0.35	0.0005-12	this work

NP: nanoparticle; GO: graphene oxide; SWCNT: single-walled carbon nanotube; G: graphene; MOF: metal-organic framework.

Table 2. Mice blood serum tests using HPLC and glucose sensor developed in this work.

Serum sample	Glucose concentration determined by HPLC	Glucose concentration determined by sensor
Serum-1	6.3 mM	6.1 mM
Serum-2	5.0 mM	4.7 mM
Serum-3	5.9 mM	5.6 mM

3.7. Mice blood serum test

In addition to the interference study, it is essential to apply the electrochemical glucose sensor in real serum test. We tested three mice blood serum samples using both high-performance liquid chromatography (HPLC) method and our Cu^{2+}-C_3N_4/MWCNT glucose sensor, and the results are summarized in Table 2. The glucose sensor shows comparable results with high accuracy and excellent reproducibility, which closely match the results from HPLC.

3. Conclusion

To conclude, by employing an ultrasonic process, we prepared a series of Cu^{2+}-doped C_3N_4 supported on MWCNT composite with different Cu^{2+} doping level and MWCNT percentage. The Cu^{2+}-doped graphitic C_3N_4 is found to be supported within MWCNT nanotube network using TEM and AFM. The atomic level doping of Cu^{2+} is suggested by the HRTEM and XRD results, which show no evidence of CuO nor $Cu(OH)_2$ composite. XRD results also confirmed the insertion of Cu^{2+} to the C_3N_4 *inter*-layer and resulting exfoliation. XPS results suggest that Cu^{2+} ions are interacting with sp^2 hybridised N species in N-$(C)_3$ structure of C_3N_4 *via* an out-of-plane on-top configuration. The EPR and *i*-V results indicate that Cu^{2+} doping and MWCNT introduction can enhance the charge carrier density and conductivity of C_3N_4. CV studies demonstrate that Cu^{2+}-doped C_3N_4 can catalyse the glucose electrooxidation, and the activity is enhanced with higher MWCNT contents. The doping level of Cu^{2+} can also affect the activity, and 12 wt% is found to be the optimal value. As a glucose sensor, Cu^{2+}(12 wt%)-C_3N_4/(5 wt%)MWCNT composite shows a high sensitivity of 929 mA/M cm^2, a large linear range (0.5 µM ~ 12 mM), low detection limit (0.35 µM) as well as short response time (< 3s). The sensor also exhibits excellent resistance to interferents such as dopamine, ascorbic acid, sucrose, and lactose. For blood serum tests, the as-prepared glucose sensor reports comparable and repeatable results, which shows the potential of such glucose sensor.

4. Acknowledgements

We acknowledge the support from the Innovation and Technology Commission of Hong Kong and the Hong Kong Polytechnic University. K.-Y. Wong acknowledges the support from the Patrick S.C. Poon Endowed Professorship.

5. References

[1] A. Brouzgou, P. Tsiakaras, *Top. Catal.* **2015**, *58*, 1311.
[2] S. Park, H. Boo, T. D. Chung, *Anal. Chim. Acta* **2006**, *556*, 46.
[3] C. Chen, Q. Xie, D. Yang, H. Xiao, Y. Fu, Y. Tan, S. Yao, *RSC Adv.* **2013**, *3*, 4473.
[4] W. Zheng, L. Hu, L. Y. S. Lee, K. Y. Wong, *J. Electroanal. Chem.* **2016**, *781*, 155.
[5] Y. Zhang, L. Su, D. Manuzzi, H. V. E. de los Monteros, W. Jia, D. Huo, C. Hou, Y. Lei, *Biosens. Bioelectron.* **2012**, *31*, 426.
[6] J. Zhang, J. Ma, S. Zhang, W. Wang, Z. Chen, *Sensors Actuators, B Chem.* **2015**, *211*, 385.
[7] N. Quoc Dung, D. Patil, H. Jung, D. Kim, *Biosens. Bioelectron.* **2013**, *42*, 280.
[8] E. Reitz, W. Jia, M. Gentile, Y. Wang, Y. Lei, *Electroanalysis* **2008**, *20*, 2482.
[9] C. Li, Y. Su, S. Zhang, X. Lv, H. Xia, Y. Wang, *Biosens. Bioelectron.* **2010**, *26*, 903.
[10] J. M. Marioli, T. Kuwana, *Electrochim. Acta* **1992**, *37*, 1187.
[11] X. Zhang, G. Wang, W. Zhang, N. Hu, H. Wu, B. Fang, *J. Phys. Chem. C* **2008**, *112*, 8856.
[12] X. Zhang, G. Wang, X. Liu, J. Wu, M. Li, J. Gu, H. Liu, B. Fang, *J. Phys. Chem. C* **2008**, *112*, 16845.
[13] D. Jiang, Q. Liu, K. Wang, J. Qian, X. Dong, Z. Yang, X. Du, B. Qiu, *Biosens. Bioelectron.* **2014**, *54*, 273.
[14] L. C. Jiang, W. De Zhang, *Biosens. Bioelectron.* **2010**, *25*, 1402.
[15] N. Quoc Dung, D. Patil, H. Jung, D. Kim, *Biosens. Bioelectron.* **2013**, *42*, 280.
[16] W. Zheng, Y. Li, C. S. Tsang, L. Hu, M. Liu, B. Huang, L. Y. S. Lee, K. Y. Wong, *ChemElectroChem* **2017**, *4*, 2788.
[17] F. Fina, S. K. Callear, G. M. Carins, J. T. S. Irvine, *Chem. Mater.* **2015**, *27*, 2612.
[18] M. Vázquez-González, W.-C. Liao, R. Cazelles, S. Wang, X. Yu, V. Gutkin, I. Willner, *ACS Nano* **2017**, *11*, 3247.
[19] J. Liu, T. Zhang, Z. Wang, G. Dawson, W. Chen, *J. Mater. Chem.* **2011**, *21*, 14398.
[20] T. Tyborski, C. Merschjann, S. Orthmann, F. Yang, M.-C. Lux-Steiner, T. Schedel-Niedrig, *J. Phys. Condens. Matter* **2013**, *25*, 395402.
[21] B. Chai, T. Peng, J. Mao, K. Li, L. Zan, *Phys. Chem. Chem. Phys.* **2012**, *14*, 16745.
[22] F. Dong, L. Wu, Y. Sun, M. Fu, Z. Wu, S. C. Lee, *J. Mater. Chem.* **2011**, *21*, 15171.
[23] T. I. T. Okpalugo, P. Papakonstantinou, H. Murphy, J. McLaughlin, N. M. D. Brown, *Carbon N. Y.* **2005**, *43*, 153.
[24] M. C. Biesinger, L. W. M. Lau, A. R. Gerson, R. S. C. Smart, *Appl. Surf. Sci.* **2010**, *257*, 887.
[25] J. Fang, H. Fan, M. Li, C. Long, *J. Mater. Chem. A* **2015**, *3*, 13819.
[26] Q. Liu, T. Chen, Y. Guo, Z. Zhang, X. Fang, *Appl. Catal. B Environ.* **2017**, *205*, 173.
[27] S. M. Lyth, Y. Nabae, S. Moriya, S. Kuroki, M. A. Kakimoto, J. I. Ozaki, S. Miyata, *J. Phys. Chem. C* **2009**, *113*, 20148.
[28] T. Yang, J. Xu, L. Lu, X. Zhu, Y. Gao, H. Xing, Y. Yu, W. Ding, Z. Liu, *J. Electroanal. Chem.* **2016**, *761*, 118.
[29] Y.-W. Hsu, T.-K. Hsu, C.-L. Sun, Y.-T. Nien, N.-W. Pu, M.-D. Ger, *Electrochim. Acta* **2012**, *82*, 152.
[30] X. Wang, C. Hu, H. Liu, G. Du, X. He, Y. Xi, *Sensors Actuators B Chem.* **2010**, *144*, 220.
[31] Y. Sun, Y. Li, N. Wang, Q. Q. Xu, L. Xu, M. Lin, *Electroanalysis* **2018**, 1.

TOC figure:

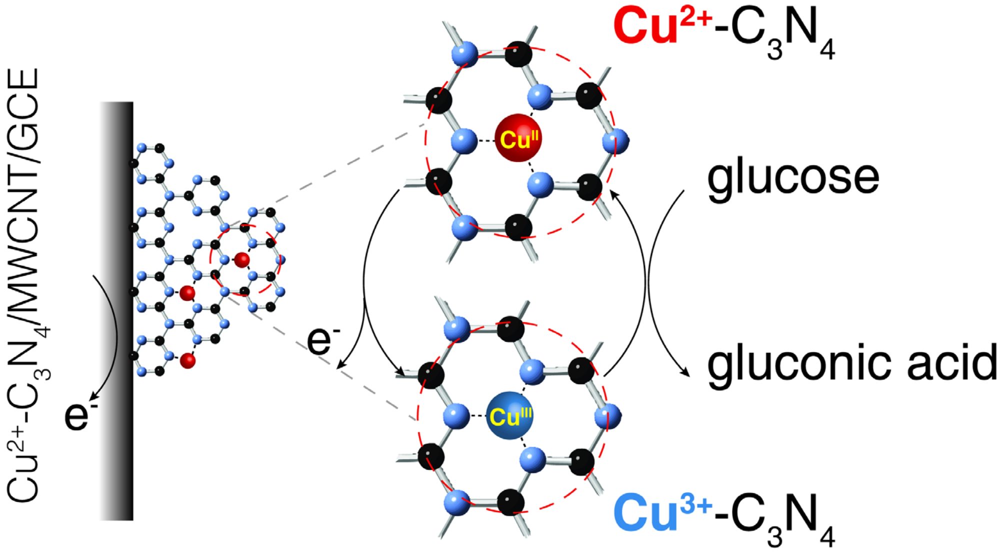

Author Names:

Weiran Zheng, Yong Li, Mengjie Liu, Chui-Shan Tsang, Lawrence Yoon Suk Lee, Kwok-Yin Wong

(W. Zheng, Y. Li, M. Liu, C.-S. Tsang, L. Y. S. Lee, K.-Y. Wong)